Infrared and Ultraviolet Spectroscopy of Water-Containing Clusters of Indole, 1-Methylindole, and 3-Methylindole

Joel R. Carney and Timothy S. Zwier*

Department of Chemistry, Purdue University, West Lafayette, Indiana 47907-1393

Received: June 29, 1999; In Final Form: September 28, 1999

A combination of resonant two-photon ionization (R2PI), resonant ion-dip infrared spectroscopy (RIDIRS), and infrared−ultraviolet (IR−UV) hole-burning spectroscopy is used to characterize the hydrogen-bonding topologies of indole−$(water)_{1,2}$, 1-methylindole−$(water)_{1-3}$, and 3-methylindole−$(water)_1$ clusters formed and cooled in a supersonic expansion. The combination of methods provides a means of disentangling R2PI spectra that contain contributions from more than one species in the same mass channel due either to fragmentation or to the presence of conformational isomers. Density functional theory calculations (DFT Becke3LYP/6-31+G*) of the structures, harmonic vibrational frequencies, and infrared intensities provide a basis for distinguishing which structures are observed experimentally. The clusters studied exhibit a range of solvation structures around indole. In the indole−$(water)_1$ and 3-methylindole−$(water)_1$ complexes, the RIDIR spectra provide a benchmark frequency shift for the N−H···OH_2 H-bonds in these structurally well-characterized complexes. In indole−$(water)_2$, the two water molecules form a water dimer bridge between the N−H H-bond donor site and the indole π cloud acceptor site. For 1-methylindole−$(water)_n$ clusters, the N−H H-bonding site is blocked, favoring structures in which water acts as an H-bond donor to the indole π cloud. The RIDIR spectra show water to be π-bound either as a single molecule ($n = 1$), a water dimer ($n = 2$), or a water trimer cycle ($n = 3$). Two isomers of 1-methylindole−$(water)_3$ with similar but highly entangled UV spectra are distinguished and assigned using IR−UV hole-burning spectroscopy. The isomers differ in the orientation of the H-bonds (clockwise or counterclockwise) in the water trimer cycle relative to 1-methylindole, effectively freezing out the two chiral structures of the cyclic water trimer. After the H-bonding topologies of these clusters are assigned, their electronic frequency shifts and Franck−Condon profiles are reevaluated in terms of the $^1L_a-^1L_b$ character of the observed transitions. A coherent explanation of these data can be made without invoking $^1L_a-^1L_b$ energy reversal.

I. Introduction

Tryptophan (Trp) dominates the near-UV fluorescence of most proteins.[1,2] The sensitivity of its ultraviolet emission spectrum and fluorescence lifetime to its local environment makes it a useful internal fluorescent probe of protein structure and solvent accessibility.[2−5] Recent studies have highlighted the crucial role played by the two close-lying excited states, ^1L_a and ^1L_b, responsible for the ultraviolet emission of Trp.[6] However, these states respond differently to polar solvents and to conformational changes in the structure of Trp itself, complicating simple interpretations of the observed fluorescence properties and impeding a molecular-scale interpretation of the effects.[7] In solution, the presence of multiple, interconverting conformations of Trp occurs in a dynamic, locally heterogeneous solvent environment.[8−10] Even in the gas phase, the presence of different ground-state conformations of the aromatic amino acid produces multiexponential fluorescence decays.[11,12] As a result, many past studies have turned to simpler analogues of Trp in an attempt to clarify the observed behavior.

The aromatic chromophore responsible for tryptophan photophysics is indole, whose electronic spectroscopy and photophysics have received much attention.[13−21] Recent experimental work by Callis and co-workers[16] has located the ^1L_a origin 1400 cm^{-1} above the $S_1(^1L_b) \leftarrow S_0$ origin. Numerous substituted indoles with different $^1L_a-^1L_b$ energy gaps, including those examined in the present work, have been studied as a means of controlling and varying the relative energies of the two excited states.[22−25]

Alternatively, one can change the $^1L_a-^1L_b$ energy spacing by exposing the chromophores to different solvent environments. From such work, a coherent explanation of solvent effects is beginning to emerge. Polar solvents are expected to stabilize the ^1L_a state more dramatically than the ^1L_b state of indole because the former has a dipole moment (5.4 D) much larger than the latter (3.5 D).[3] Consistent with Kasha's rule, if stabilization of ^1L_a is sufficient to reorder the ^1L_a and ^1L_b states, emission will occur from the former in environments where it is lower than ^1L_b. Because of the solvent reorganization in response to electronic excitation, ^1L_a emission is characterized by broad, red-shifted emission, while the less-sensitive ^1L_b emission is not shifted and is comparatively sharp.

It has been proposed[26,27] that polar solvent molecules bound to the π cloud of indole are particularly important in selectively stabilizing the ^1L_a state. In testing this molecular-scale interpretation, the study of gas-phase molecular clusters offers a powerful alternative to bulk solution-phase studies because the clusters incorporate solvent molecules in well-defined solute−$(solvent)_n$ structures. As a result, several investigations of the electronic spectroscopy of indole−$(solvent)_n$ clusters have been undertaken.[22,26−34] Water is the most common solvent studied

* To whom correspondence should be addressed.

10.1021/jp992222t CCC: $18.00
Published on Web 11/04/1999

in these clusters because of its relevance to the natural environment of amino acids.

Early work on indole−(water)$_n$ clusters identified ultraviolet transitions due to two species that were subsequently assigned as two isomers of indole−(water)$_1$ on the basis of R2PI mass analysis and the characteristic signatures of their vibronic spectroscopy.[26,34,35] One isomer has an ultraviolet spectrum with an $S_1 \leftarrow S_0$ electronic frequency shift of -132 cm^{-1} and little intermolecular Franck−Condon activity. These are signatures of a ^1L_b excited state, with only modest stabilization of the excited state and little solvent reorganization upon electronic excitation. This isomer was assigned as one in which water attaches as H-bond acceptor at indole's N−H site. Subsequent high-resolution spectroscopy[31] confirmed this structure, provided a quantitative heavy-atom separation for the H-bond (R_{N-O} = 3.07 Å), and characterized the hindered internal rotation of the water molecule about the N−H···O axis.

The second species possesses an electronic frequency shift of -452 cm^{-1} and long intermolecular progressions. Short and Callis have recently reviewed the colorful history of the assignments for this band system.[33] Most of the recent work assigned these bands to a second indole−water isomer in which the water molecule binds as a H-bond donor to indole's π cloud.[22,26,27] The spectroscopy was consistent with incipient ^1L_a excited-state character, suggesting the dramatic consequences a single water molecule could have on the electronic structure of indole. Subsequent attempts to obtain a high-resolution spectrum of this red-shifted complex failed.[36] In recent work,[28] our group has recorded the resonant ion-dip infrared spectrum of this second species. It was thereby reassigned as the indole−W_2 (W is water) cluster appearing in the indole−(water)$_1^+$ mass channel in R2PI by virtue of near-complete fragmentation by loss of a single water molecule following photoionization. When compared with DFT calculations, the RIDIR spectrum was assigned to an indole−W_2 structure in which the water dimer acts as a bridge between the N−H group on indole and the π cloud. Following this reassignment, Short and Callis[33] have shown unequivocally that the two-photon polarized fluorescence excitation and dispersed emission spectra of both indole−W_1 and indole−W_2 occur from a ^1L_b excited state, casting further doubt on a simple interpretation of the effects of π-cloud binding on the excited states of indole.

This paper presents new results on the ultraviolet and infrared spectroscopy of small water clusters with indole, 1-methylindole (1MI), and 3-methylindole (3MI). The present results build on the earlier communication on indole−W_n[28] clusters in several ways. First, the signal-to-noise and resolution of the infrared data on the indole−W_n clusters are improved and analyzed in more detail. Second, analogous studies of 1-methylindole−(water)$_n$ clusters (1MI) are undertaken. One anticipates that a π···solvent interaction will be forced by methylation of the strong, N−H hydrogen-bonding site of indole. The $S_1 \leftarrow S_0$ origin of 1MI lies 700 cm^{-1} (34 544 vs 35 241) to the red of indole. Previous R2PI studies[22,26] of gas-phase 1MI−W_n clusters led to assignments of all R2PI features in the 1MI−W_1^+ mass channel to a π-bound 1MI−W_1 species. The spectrum so obtained extends over 400 cm^{-1} to the red of the monomer origin and exhibits dense, extensive intermolecular band structure. This would seem to confirm the theory that π H-bonding by water is sufficient to reverse the energy ordering of ^1L_a and ^1L_b states. However, in the present work, a combination of RIDIR spectroscopy and IR−UV hole-burning leads to a reassignment of the 1MI−W_n cluster spectra and necessitates a reevaluation of the deductions arising from them regarding ^1L_a character.

Finally, we present the RIDIR spectrum of the 3-methylindole−(water)$_1$ complex (3MI−W_1). Methylation now occurs at C3 (see, for example, ref 22 for indole atom numbering), which is the same position that the peptide side chain of Trp attaches. While this leaves open the N−H site on indole, it also decreases the ^1L_a−^1L_b energy gap to about 400 cm^{-1},[24] suggesting that water solvation could more easily reverse the energy ordering of the excited states.

II. Methods

A. Experimental. Our experimental setup has been described elsewhere[37] in detail. Briefly, cold gas-phase clusters are produced in a supersonic expansion through a pulsed valve with a diameter of 0.8 mm operating at 20 Hz. A 70% neon, 30% helium mixture is used as a carrier gas at a backing pressure of 1.5 bar. Indole (or a derivative) and water vapor each constitute about 0.02% of the gas pulse. The expansion is skimmed before the clusters enter the ion source region of a linear time-of-flight mass spectrometer.

This work employs a combination of methods, which have as their starting point mass-selected, resonant two-photon ionization (R2PI) spectroscopy. The doubled output of a Nd:YAG-pumped dye laser operating at 20 Hz is used as the ionization source, with mass selection via linear time-of-flight methods. Typical UV output is 0.5 mJ/pulse (using rhodamine 590 or a 590/610 dye mixture), which is left unfocused to minimize fragmentation of the clusters.

To record the size and conformer-specific infrared spectrum of a single cluster, the mass and wavelength selectivity offered by R2PI is utilized as part of a double-resonance scheme, which we have described previously,[38] called resonant ion-dip infrared spectroscopy (RIDIRS). Here, the infrared output of a seeded Nd:YAG-pumped optical parametric oscillator operated at 10 Hz is spatially overlapped with the ionization laser, preceding the UV by 200 ns. The UV source is fixed to a desired vibronic transition, which creates a constant ion signal, and the IR is scanned. When the selected cluster is resonant with an IR transition, its ground-state population, and thus the constant ion signal, is depleted. The difference between the ion signal with and without the IR present is monitored via active baseline subtraction and is interfaced to a personal computer.

The R2PI spectra observed in this work are often congested because they arise from more than one species present in a given mass channel. IR−UV hole-burning is a spectroscopic tool, which identifies all the UV vibronic transitions due to a single species in the R2PI spectrum. To achieve such selection, a convention opposite that of RIDIRS is used. Here, the IR is fixed to a unique absorption while the UV laser is scanned. As in RIDIRS, the difference in ion intensity with and without the IR laser present is recorded using active baseline subtraction. All vibronic transitions that arise from the ground-state responsible for the unique IR absorption will show up as depletions in the UV hole-burning spectrum. Both RIDIR and hole-burning spectra are plotted as positive-going signals in this work.

B. Computational. Density functional theory calculations of the structures, dipole moments, binding energies, harmonic vibrational frequencies, and infrared intensities were carried out in Gaussian 94[39] using the Becke3LYP functional with a 6-31+G* basis set.

The DFT Becke3LYP/6-31+G*(5d)[40] level of theory has been used in several recent studies[28,41] of H-bonded clusters to compare with experimental results. The computed harmonic

vibrational frequencies and infrared intensities at this level of theory serve as a quantitatively useful guide in assigning spectra while maintaining the necessary computational efficiency for studying clusters of this size (>10 heavy atoms).

Full optimizations of the cluster structures were carried out from a range of starting geometries chosen to explore the various minima expected for a given structure. Optimizations employed tight convergence and scaled steps on the potential energy surface about the minima to carefully extract the lowest-energy structures. The location of true minima was confirmed by the lack of imaginary frequencies in the vibrational frequency calculations.

Binding energies for the clusters, both with and without zero-point energy correction, were determined. Zero-point energy corrections are performed by Gaussian on all reported binding energies using the harmonic frequencies of the modes. In the 1:1 complexes of indole and 1-methylindole with water, corrections have also been made for basis set superposition error to better compare with the experimental measurements of Mons and co-workers reported in the adjoining paper.[42]

Calculated frequencies are scaled by a factor of 0.9775, which minimizes the difference between the experimental and calculated frequencies in the O−H and N−H stretch regions for the entire set of structures identified experimentally.

III. Results and Analysis

A. Calculations. The DFT calculations are used in several ways in the present work. First, they identify various low-lying minimum-energy structures for the clusters of interest. Second, they provide predictions of the energy ordering of these structures. Third, the computed harmonic vibrational frequencies and infrared intensities are used to simulate infrared spectra for the clusters. These, in turn, serve as a basis both for distinguishing which structures are observed experimentally and for analyzing the spectroscopic consequences of the H-bonded structures so identified.

Given the size and functionality of indole, one can anticipate several different binding sites for water to indole: as acceptor at the N−H site; as H-bond donor to the π cloud at the pyrrole ring and at the phenyl ring. In the larger clusters, more than one structure for the water clusters attached at these points can also be imagined. As a result, we have carried out a number of exploratory calculations to locate minima at these positions. While a detailed discussion of the structures will await assignment of the experimental spectra, a summary of the structural predictions of the calculations is worthwhile here.

Figure 1 is a presentation of the various minima calculated in this study for indole−$(water)_{1-3}$, 1-methylindole−$(water)_{1-3}$, and 3-methylindole−$(water)_{1,2}$ clusters. Table 1 summarizes the binding energies (both corrected and uncorrected for zero-point energy) and dipole moments of the structures pictured in Figure 1. For Ind−W_1 (Ind is indole; Figure 1a, structures **1**−**3**), minima are found for all three of the anticipated binding sites on indole: the pyrrole N−H, the pyrrole π cloud, and the phenyl ring π cloud. The N−H···OH_2 H-bond is calculated to be almost twice as strong as either π interaction. Given the calculated energy separation between the N−H and π-bound sites, searches for structures of larger Ind−W_n clusters were restricted to those involving a primary N−H···OH_2 H-bond in the input geometry. Two isomers of Ind−W_2 are identified (Figure 1a, structures **4** and **5**) that form a bridge between the N−H site and π-cloud, both of which bind to the indole π cloud between the C6 and C7 positions on the phenyl ring. A similar structure was attempted in which the secondary π interaction was directed toward the pyrrole ring of indole. This species optimized to one of the previously mentioned minima. An even longer bridge is calculated to be the minimum energy structure of Ind−W_3 (Figure 1a, structure **6**). The extended length of this W_3 bridge makes possible a secondary interaction with the π cloud of indole near the C3 position on the pyrrole ring, which is known to be an electron-rich region of indole.[26] This structure is calculated to be much more stable than the two Ind−W_3 cycles (structures **7** and **8**) that are shown in Figure 1a.

The only minimum found for 1MI−W_1 incorporates water in a π H-bond to indole at the C3 position on the pyrrole ring (Figure 1b, structure **1**). All attempts at finding a second minimum with a π H-bond to the phenyl portion of indole were unsuccessful, indicating that there is no barrier to movement between the two rings in 1MI at the present level of theory.

Three different minima are calculated for 1MI−W_2, all of which include a water dimer bound to indole's π cloud but differing in the orientation of the water dimer relative to indole. The lowest-energy structure (Figure 1b, structure **2**) shows a water dimer in which the acceptor water participates in a π H-bond near C3 while the donor water interacts weakly with the methyl group on the pyrrole ring. A second minimum (Figure 1b, structure **3**) orients the dimer along the long axis of indole, with a π H-bond near C6. The third isomer (Figure 1b structure **4**) retains the π H-bond at C3 but rotates the water dimer so that the donor water projects away from the pyrrole ring.

One can imagine two structural types for 1MI−W_3 containing either a water trimer *chain* bridging the two π clouds of 1MI or a water trimer *cycle*. All attempts at locating a W_3 chain converged to the more stable cyclic structures. Interestingly, two cyclic 1MI−W_3 minima were located, both of which possessed π H-bonds in the proximity of the C3 and C6 positions of 1MI. The two isomers differ in the directionality of the water−water hydrogen bonds in the cycle relative to the 1MI molecule, either "clockwise" (Figure 1b, structure **5**) or "counterclockwise" (Figure 1b, structure **6**). These two similar structures were investigated with some foresight because experimental evidence calls for two closely similar structural isomers for 1MI−W_3.

Structures **1** and **2** in Figure 1c are the N−H bound minima for 3MI−W_1 and 3MI−W_2 clusters that correspond to the indole−W_n structures **1** and **5** in Figure 1a. As anticipated, their geometries are very similar. Extensive calculations on larger 3MI−W_n clusters were not pursued because of the lack of experimental data on these larger clusters.

Table 2 presents the key structural parameters of the lowest-energy structures computed for the clusters. Here, we have focused attention on the parameters of most relevance for hydrogen bonding, namely, the OH and NH bond lengths, heavy-atom separations (N/O or O/O) in the H-bonds, and selected H-bond angles.

Finally, the hydride stretch vibrational frequencies of the experimentally relevant structures are collected in Table 3 for comparison with experimental results. Experimental and calculated (scaled) IR frequencies are compared in the first section. Then wavenumber shifts are reported, relative to the free N−H stretch of indole or the average between the symmetric and antisymmetric O−H stretches of water monomer. The modes are described in the last column.

The calculations provide some helpful generalizations in analyzing clusters of indole and its substituted analogues. First, one sees a significant energetic preference for binding water at the N−H site of indole over its π cloud when both are

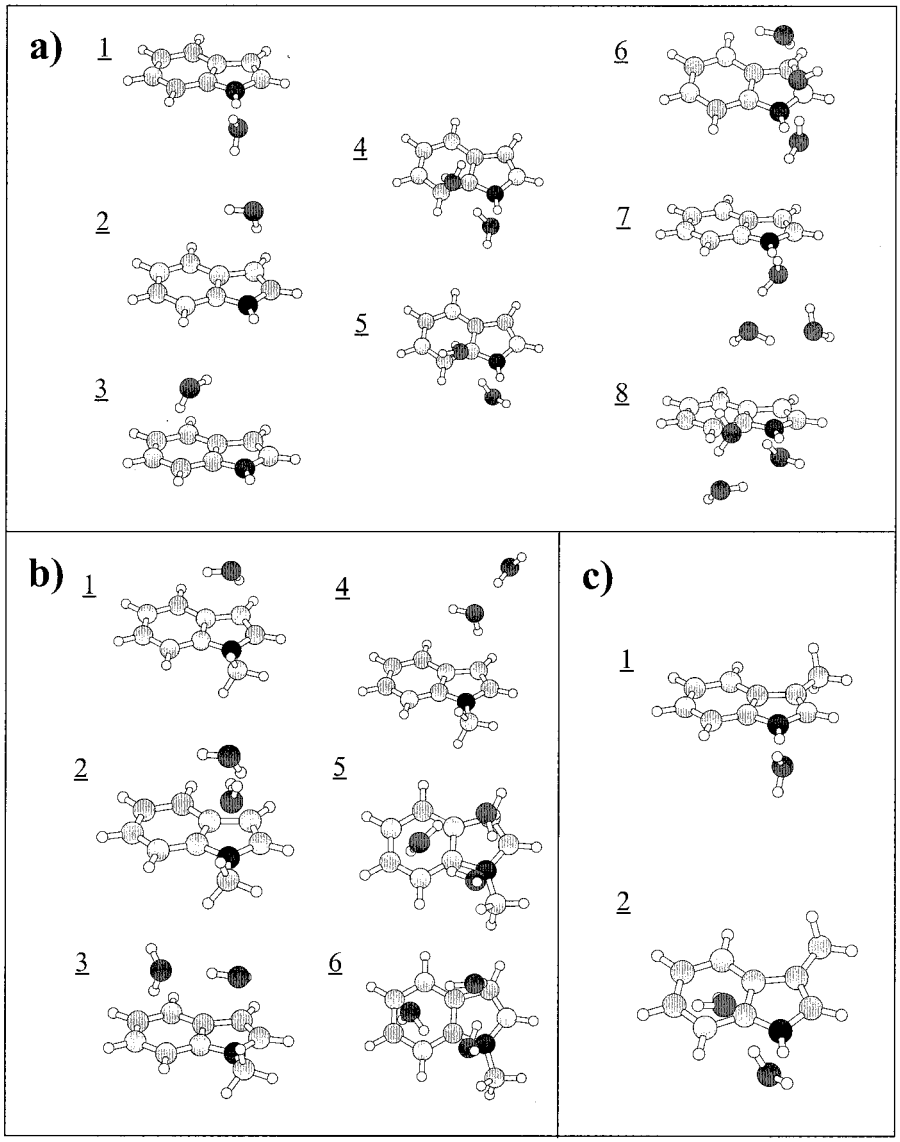

Figure 1. Pictorial summary of the calculated structural minima for (a) Ind−W_n (n = 1−3), (b) 1MI−W_n (n = 1−3), and (c) 3MI−W_n (n = 1, 2).

accessible. Second, larger Ind−W_n clusters tend to create H-bonded bridges between the N−H site and π cloud of indole. The π interaction is near the phenyl moiety in 1:2 clusters, while a W_3 chain is able to reach back to interact with the pyrrole ring, near C3. Third, when π H-bonds are formed, they preferentially occur at the C3 position on the pyrrole ring and secondarily at the C6 position when the C3 site cannot be reached (as in Ind−W_2). The 1:1 clusters of indole and 1MI with water will be discussed more completely in the adjoining paper by Mons and co-workers.[42]

B. Experimental. *1. Indole−(Water)$_n$, n = 1, 2.* R2PI spectra in the Ind^+ and Ind−W_1^+ mass channels in the origin region of the $S_1 \leftarrow S_0$ transition of indole are shown in Figure 2. The R2PI spectra are similar to those recorded by other groups previously,[22,26,32,35] including our own.[28] The monomer origin appears at 35 241 cm^{-1}. The corresponding origins of Ind−W_1 and Ind−W_2 are located 132 and 452 cm^{-1} to the red of the indole monomer, respectively, as indicated in the figure. The assignments of transitions due to Ind−W_1 and Ind−W_2 are the revised assignments reported in our earlier communication.[28] Transitions assigned to Ind−W_2 appear also weakly in the Ind−W_2^+ mass channel. However, fragmentation of the ionized cluster following photoionization is efficient, making proper assignment in the absence of definitive structural evidence difficult.

Ind and Ind−W_1 exhibit strong origins with smaller vibronic features at higher frequencies. Conversely, long FC progressions in a 34 cm^{-1} intermolecular mode of Ind−W_2 are built off the origin and off an intermolecular fundamental of 48 cm^{-1}. The progressions cover a 300 cm^{-1} region, indicating a substantial change in geometry between S_0 and S_1 along the 34 cm^{-1} mode.[43] The electronic origins and wavenumber shifts of the Ind−W_n clusters are gathered together in Table 4 with those from all the other clusters studied in this paper.

RIDIR spectra of Ind, Ind−W_1, and Ind−W_2 are presented in parts a, b, and c of Figure 3, respectively. Changes in these spectra relative to those reported earlier reflect the narrower bandwidth (0.25 cm^{-1}) and higher per pulse energies of the KTA-based parametric converter. Among the improvements evident in the spectra is the increased signal-to-noise in the CH stretch region. In indole monomer, the higher-frequency fundamentals at 3140 and 3146 cm^{-1} are assigned to CH stretches on the pyrrole ring, while the phenyl ring CH stretches appear in the 3000−3100 cm^{-1} region. The latter absorptions show

TABLE 1: Binding Energies and Permanent Dipole Moments of Indole−(Water)$_n$ (n = 0−3), 1-Methylindole−(Water)$_n$ (n = 0−3), and 3-Methylindole−(Water)$_n$ (n = 0, 2) Calculated in This Study

species	BE[a] (kcal/mol)	corrected BE[b] (kcal/mol)	description of structure	permanent dipole moment[c] (D)
Ind				2.18
Ind−W_1	−6.27	−4.85/−3.63*	N−H···OH_2 (**1** in Figure 1a)	5.01
	−3.76	−2.60	π-HB to pyrrole, C3 (**2** in Figure 1a)	–
	−3.45	−2.45	π-HB to phenyl, C6 (**3** in Figure 1a)	–
Ind−W_2	−16.75	−12.55	N−H → π W_2 bridge (**4** in Figure 1a)	2.64
	−16.06	−11.72	2nd minimum (**5** in Figure 1a)	2.64
Ind−W_3	−28.84	−21.93	N−H → π W_3 bridge (**6** in Figure 1a)	1.41
	−25.60	–	N−H bound W_3 cycle (**7** in Figure 1a)	–
	−25.54	–	N−H bound W_3 cycle (**8** in Figure 1a)	–
1MI				2.46
1MI−W_1	−4.12	−2.90/−1.65*	π bound water (**1** in Figure 1b)	2.50
1MI−W_2	−14.03	−9.96	π bound W_2 (**2** in Figure 1b)	0.58
	−12.41	–	π bound W_2 (**3** in Figure 1b)	–
	−11.50	–	π bound W_2 (**4** in Figure 1b)	–
1MI−W_3	−25.57	−17.96	π bound W_3 cycle, counterclockwise (**5** in Figure 1b)	3.27
	−25.60	−18.02	π bound W_3 cycle, clockwise (**6** in Figure 1b	3.26
3MI				2.06
3MI−W_1	−6.08	−4.69	N−H···OH_2 (**1** in Figure 1c)	4.78
3MI−W_2	−15.96	−11.85	N−H π W_2 bridge (**2** in Figure 1c)	2.41

[a] Total energy of the complex minus the sum of the energies of the isolated molecules. [b] Zero-point energy correction to the binding energies. *Basis set superposition error (BSSE) correction included in the binding energies (counterpoise corrections). [c] Total dipole moment of the species.

evidence of mixing with CH bend overtones. The NH stretch of the indole monomer is the most intense absorption at 3525 cm^{-1}.

The IR spectrum of Ind−W_1 (Figure 3b) clearly reflects the known N−H···OH_2 structure for this complex.[31] The antisymmetric and symmetric stretching modes of water in the complex appear at 3747 and 3652 cm^{-1}, respectively, very near the corresponding vibrations in the water monomer (3756 and 3657 cm^{-1}). However, a large shift is observed in the NH stretch fundamental in the complex (−89 cm^{-1}), signifying the formation of an N−H···OH_2 hydrogen bond. Furthermore, the formation of the N−H···OH_2 H-bond increases the intensity of the N−H stretch fundamental in the Ind−W_1 complex (Figure 3b) relative to the indole monomer (Figure 3a), creating the false impression that the C−H stretch transitions change in intensity between the two spectra.

The RIDIR spectrum of Ind−W_1 is insensitive to certain aspects of the structure and dynamics of the complex, which have been established by Korter and Pratt.[31] In particular, their rotationally resolved ultraviolet spectrum displays a tunneling doublet (with a splitting of 0.5 cm^{-1}) due to hindered internal rotation of the water molecule about the N−H···O bond. The RIDIR spectrum we report is thus a composite of IR spectra out of both tunneling levels, since the R2PI laser does not resolve these overlapping transitions. The corresponding tunneling doublets in the vibrationally excited state are unresolved in the RIDIR spectrum.

The IR spectrum of Ind−W_2 in Figure 3c exhibits five main absorptions, which we have assigned as the five hydride stretch fundamentals of the cluster (one NH and four OH stretches). A comparison of the experimental spectrum with calculated spectra (not reproduced here) led in our prior work to the deduction that Ind−W_2 is composed of a water dimer bridge straddling between the N−H and π H-bonding sites of indole.[28] The two computed minima for Ind−W_2 (Figure 1a, structures **4** and **5**), which differ in the lone pair chosen for attachment of the N−H bound water, have calculated IR spectra that are similar enough that they cannot be used to distinguish whether structure **4** or **5** is that observed experimentally. The calculations predict a lower energy for structure **4** (Table 1), suggesting it as the preferred possibility.

The improved signal-to-noise of the spectrum in Figure 3c clarifies the presence of several weak bands appearing in the midst of the hydride stretch fundamentals. The bands at 3424 and 3505 cm^{-1} are 23 and 17 cm^{-1} above the two mixed NH/OH stretch fundamentals at 3402 and 3488 cm^{-1}, respectively. It seems likely that these bands are simple combination bands involving a hydride stretch and low-frequency intermolecular vibrations that swing the water dimer bridge along the indole π cloud.

As the inset in Figure 3c shows, the additional structure is also now clearly evident in the π H-bonded OH stretch fundamental centered at 3708 cm^{-1}. Here, the likely cause of the additional structure is Fermi resonance mixing of this fundamental with hydride stretch−intermolecular combination bands built off of lower-frequency hydride stretch fundamentals. Why such Fermi resonance mixing is selectively present on this band is unclear.

2. 1-Methylindole−(Water)$_n$, n = 1−3. Methyl substitution at the NH site of indole blocks the preferred binding site for attachment of water. The anticipated attachment point for water is thereby shifted to the π cloud of indole in the 1MI−W_n clusters. R2PI spectra in the 1MI−W_n^+ (n = 0−2) mass channels are shown in Figure 4. The positions of the $S_1 \leftarrow S_0$ origins of 1MI−W_1 (−95 cm^{-1}), 1MI−W_2 (−417 cm^{-1}), and two isomers of 1MI−W_3 (−109 and −95 cm^{-1}) are labeled in the spectrum. The assignments are based on the RIDIR and IR−UV hole-burning spectra, which follow.

Efficient fragmentation by loss of a single water is once again apparent in the R2PI spectra of 1MI−W_n. The spectrum in the 1MI parent mass channel (Figure 4a) was recorded without water present in the expansion. However, the transitions assigned to 1MI−W_1 (stretching from −95 to +41 cm^{-1} in the 1MI−W_1^+ mass channel) can be readily observed in the $1MI^+$ mass channel when water is present. Similar fragmentation is apparent in 1MI−W_2, where comparable ion intensities appear in both 1MI−W_1^+ (Figure 4b) and 1MI−W_2^+ (Figure 4c) mass channels in the −417 to −130 cm^{-1} region. The combined

TABLE 2: Summary of the Calculated N−H and O−H Bond Distances, Heavy-Atom Separations, and Selected Bond Angles Calculated at the DFT Becke3LYP/6-31+G* Level of Theory

species	hydride dist[a] (O−H/N−H)	description	heavy-atom dist or bond angle[b]	description
Ind	1.009	N−H		
Ind−W_1	1.016	N−H	2.985	N···O
	0.969	O−H	179.6*	N−H−O
Ind−W_2 (I)[c]	1.019	N−H	2.887	N···O(1)
	0.968	free O−H (1)	2.804	O(1)···O(2)
	0.984	SD O−H (1)	150.9*	N−H−O(1)
	0.970	free O−H (2)	163.8*	O(1)−H−O(2)
	0.976	π O−H (2)		
Ind−W_2 (II)[c]	1.020	N−H	2.911	N···O(1)
	0.968	free O−H (1)	2.801	O(1)···O(2)
	0.984	SD O−H (1)	153.1*	N−H−O(1)
	0.969	free O−H (2)	161.6*	O(1)−H−O(2)
	0.976	π O−H (2)		
Ind−W_3[d]	1.024	N−H	2.855	N···O(1)
	0.968	free O−H (1)	2.754	O(1)···O(2)
	0.989	SD O−H (1)	2.778	O(2)···O(3)
	0.968	free O−H (2)	158.7*	N−H−O(1)
	0.989	SD O−H (2)	170.1*	O(1)−H−O(2)
	0.970	free O−H (3)	178.2*	O(2)−H−O(3)
	0.979	π O−H (3)		
3MI	1.008	N−H		
3MI−W_1	1.016	N−H	2.989	N···O
	0.970	Free O−H	179.4*	N−H−O
3MI−W_2[c]	1.020	N−H	2.918	N···O(1)
	0.968	free O−H (1)	2.803	O(1)···O(2)
	0.984	SD O−H (1)	153.0*	N−H−O(1)
	0.969	free O−H (2)	161.9*	O(1)−H−O(2)
	0.976	π O−H (2)		
1MI−W_1	0.970	Free O−H		
	0.973	π O−H		
1MI−W_2[e]	0.971	free O−H (1)	2.827	O(1)···O(2)
	0.977	π O−H (1)	172.2*	O(1)−H−O(2)
	0.968	free O−H (2)		
	0.983	SD O−H (2)		
1MI−W_3 (I)[f]	0.974	π O−H (C3)	2.857	O(C3)···O(meth)
	0.981	SD O−H (C3)	2.804	O(C3)···O(C6)
	0.969	free O−H (meth)	2.748	O(C6)···O(meth)
	0.991	SD O−H (meth)	156.6*	O(meth)−H−O(C6)
	0.972	π O−H (C6)	149.9*	O(C6)−H−O(C3)
	0.985	SD O−H (C6)	148.3*	O(C3)−H−O(meth)
1MI−W_3 (II)[f]	0.974	π O−H (C3)	2.747	O(C3)···O(meth)
	0.985	SD O−H (C3)	2.805	O(C3)···O(C6)
	0.969	free O−H (meth)	2.861	O(C6)···O(meth)
	0.991	SD O−H (meth)	157.1*	O(meth)−H−O(C3)
	0.972	π O−H (C6)	149.8*	O(C3)−H−O(C6)
	0.981	SD O−H (C6)	148.3*	O(C6)−H−O(meth)

[a] OH/NH bond distances in angstroms. [b] Heavy-atom separations in angstroms. * denotes hydrogen bond angles in degrees (180 = linear H-bond). [c] (1) = water bound to NH group of indole. (2) = second water in chain, π-hydrogen-bound to indole. [d] (1) = water bound to NH group of indole. (2) = second water in chain. (3) = third water in chain, π-hydrogen-bound to indole. [e] (1) = π-hydrogen bound water. (2) = second water in the complex, next to methyl group. [f] (C3) = water molecule nearest the no. 3 carbon position of 1MI. (C6) = water molecule nearest the no. 6 carbon position of 1MI. (meth) = water molecule nearest the methyl group of 1MI.

consequences of this fragmentation, the extensive intermolecular Franck−Condon activity observed, and the presence of multiple isomers lead to a complex, highly congested set of R2PI spectra.

In disentangling such congested R2PI spectra, the following procedure was used. First, RIDIR spectra were taken of selected strong features suspected of being due to different species. Second, from the RIDIR spectra, unique IR absorptions could be identified that could serve as the basis of IR−UV hole-burning. Third, if some transitions were missing from the hole-burning spectra, these could then serve as monitoring transitions for new RIDIR scans, which thereby identify new species. This procedure led to the identification of transitions due to three contributing species in the 1MI−W_2^+ mass channel: the red-shifted transitions due to 1MI−W_2 and two close-lying sets of transitions beginning at −95 and −109 cm^{-1} due to two 1MI−W_3 isomers.

RIDIR spectra of 1MI−W_n (n = 1−3) clusters are presented in Figure 5−7, respectively. They are compared with the calculated vibrational frequencies and infrared intensities of the lowest-energy structures identified in the calculations. The calculated stick spectra in the hydride stretch region are shown in the top half of each figure, and experimental data are plotted below for comparison. Pictures of the calculated structures for 1MI−W_1 and 1MI−W_2 are included as insets in Figures 5 and 6. The two conformations of 1MI−W_3, which correspond to the calculated spectra in parts a and b of Figure 7, are presented in Figure 8.

(a) 1MI−W_1. In the RIDIR scan of 1MI−W_1 in Figure 5b, the ion signal for the complex was monitored in the $1MI^+$ mass channel, where the ion signal was nearly free from contamination from other species. The most intense UV feature (at −29 cm^{-1}) was chosen as RIDIR monitoring transition in order to

TABLE 3: Summary of Experimental and Calculated N−H and O−H Vibrational Frequencies of Indole−(Water)$_n$ (n = 0, 2), 1-Methylindole−(Water)$_n$ (n = 0−3), and 3-Methylindole−(Water)$_n$ (n = 0, 1)

	vibrational frequency[a]		wavenumber shift[a]		
species	exptl[b]	calcd[c]	N−H[d]	O−H[e]	description
Ind	3525	3585	0		N−H
Ind−W_1	3747	3764		+40	O−H AS
	3652	3650		−55	O−H SS
	3436	3478	−89		N−H
Ind−W_2 (A)	3725	3738		+18	w2 O trans
	3708	3724		+1	w2 O−H AS
	3585	3575		−122	w2 O−H SS
	3488	3447	−37		N−H, O−H bend (sym)
	3402	3414	−123		N−H, O−H bend (asym)
Ind−W_2 (B)		3735			
		3730			
		3589			
		3450			
		3399			
1MI−W_1	3704	3731		−3	free O−H
	3615	3609		−92	π O−H
1MI−W_2	3717	3609		10	free O−H
	3676	3712		−31	O−H AS (π water)
	3599	3561		−108	O−H SS (π water)
	3498	3448		−209	SD O−H
1MI−W_3 (I)	3705	3725		−2	free O−H
	3639	3670		−68	π O−H
	3630	3643		−77	π O−H
	3548	3499		−123	SD O−H
	3491	3425		−216	SD O−H
	3370	3302		−337	SD O−H
1MI−W_3 (II)	3705	3726		−2	free O−H
	3646	3675		−61	π O−H
	3616	3632		−91	π O−H
	3560	3499		−147	SD O−H
	3469	3427		−238	SD O−H
	3370	3301		−337	SD O−H
3MI	3526	3589	+1		N−H
3MI−W_1	3747	3764		+40	O−H AS
	3652	3650		−55	O−H SS
	3442	3482	−83		N−H

[a] Frequencies given in wavenumbers (cm^{-1}). [b] Peak positions from RIDIR spectra. [c] Calculated frequencies after scaling, scaling factor = 0.9775. [d] Experimental frequency shift, in wavenumbers, relative to the experimental N−H stretch fundamental of indole (3525 cm^{-1}). [e] Experimental frequency shift, in wavenumbers, relative to the experimental mean of the symmetric and antisymmetric stretch fundamentals of water monomer (3706.5 cm^{-1}). [f] Hydride stretch mode description: N−H = N−H stretch of indole monomer; O−H AS = the antisymmetric stretch of water; O−H SS = the symmetric stretch of water; (π water) = π-hydrogen bound water molecule.

maximize the ion signal for the depletion experiment. The experimental spectrum shows characteristic absorptions due to a π-bound water molecule, with OH stretch fundamentals at 3704 and 3615 cm^{-1}, about 40−50 cm^{-1} shifted down in wavenumber from the symmetric and antisymmetric stretch modes of free water (3657/3756 cm^{-1}). The calculated (scaled) stick spectrum (Figure 5a) nicely reproduces the positions and relative intensities of the experimental spectrum. According to the calculations, the π hydrogen bond is directed toward the C3 position of 1MI, which has been predicted to be the most likely binding site of indole's π cloud.[26] The experimental spectrum does not constrain this position nor does it give any detailed insight into the orientation or floppiness of the complex.

(b) 1MI−W_2. The ion signal for the RIDIR spectrum of 1MI−W_2 (Figure 6b) was monitored in the 1MI−W_1^+ mass channel. The most intense UV feature (−183 cm^{-1}) in the spectral region from −417 to −131 cm^{-1} was chosen to maximize the ion signal for the depletion experiment. The spectrum unambiguously identifies the carrier as 1MI−W_2 via its four OH stretch fundamentals. The general appearance of the spectrum is reminiscent of that obtained previously for benzene−(water)$_2$.[44] Consistent with a π H-bound water dimer, the OH stretch fundamentals of the donor water molecule in the water dimer appear at 3498 cm^{-1} (H-bonded OH) and 3717 cm^{-1} (free OH). The acceptor water in the water dimer has absorptions at 3676 and 3599 cm^{-1}.

The calculated IR spectrum (Figure 6a) confirms this picture, faithfully reproducing the spacing and relative intensities of the OH stretch transitions. The π-hydrogen bond is directed toward the C3 position of 1MI, and a methyl···O−H_2 interaction seems to attract the lone pair of electrons on the non-π-hydrogen-bound water.

Hole-burning scans in the 1MI−W_1^+ mass channel are shown in parts b and c of Figure 9, with the corresponding R2PI spectrum reproduced in Figure 9a. The IR output used to hole-burn was fixed at 3599 and 3615 cm^{-1} for traces in parts b and c, respectively. These hydride stretch transitions were chosen because they were intense, sharp, nonoverlapping IR features that could be clearly used to differentiate vibronic signatures of 1MI−W_1 and 1MI−W_2. The hole-burning scans cleanly separate into two subspectra due to 1MI−W_1 and 1MI−W_2. This confirms the assignment of the ultraviolet transitions and highlights the UV spectra of each type free from interference from one another.

(c) 1MI−W_3. Two unique RIDIR spectra were obtained from the congested set of transitions spanning the range from −109 to +131 cm^{-1} in the 1MI−W_2^+ mass channel. Their IR spectra are very similar (parts c and d of Figure 7) but distinguishable

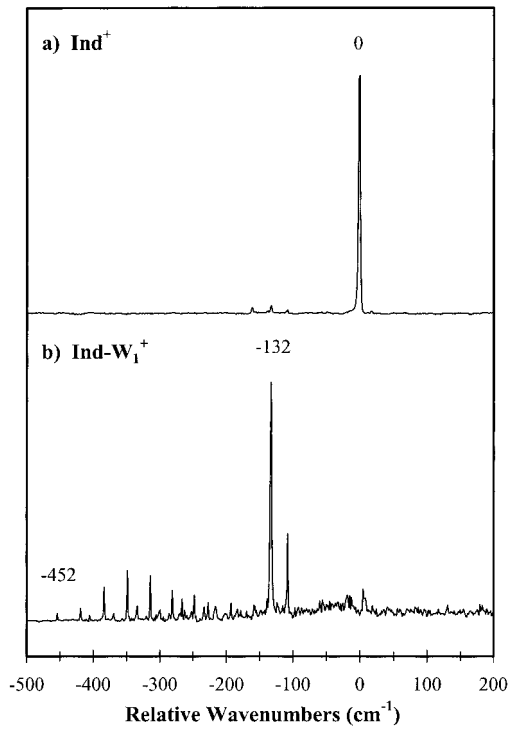

Figure 2. One-color resonant two-photon ionization spectra while monitoring the Ind^+ (a) and $Ind-W_1^+$ (b) mass channels in the $S_1 \leftarrow S_0$ origin region of indole. The zero of the relative wavenumber scale is the origin of indole (35 241 cm^{-1}). The previously assigned origins of Ind, $Ind-W_1$ (-132 cm^{-1}), and $Ind-W_2$ (-452 cm^{-1}) are labeled.

in the hydride stretch region. Both spectra show the requisite six OH stretch fundamentals expected of $1MI-W_3$. Two limiting H-bonding topologies seem most likely for $1MI-W_3$: a π-bound W_3 cycle and a π-bound W_3 chain. The former structure would have three OH···O H-bonded stretches, while the latter would have two. The number and strength of the π H-bonds formed in either structure are difficult to predict. Since the experimental spectra show no obvious separation between water-bound and π-bound OH stretches, the distinction between a W_3 cycle and chain is not easily made apart from calculation. However, the great similarity between the two RIDIR spectra suggests that a more subtle difference in structure distinguishes the two isomers.

A resolution of this quandary followed the realization that W_3 cycles, which differ in the direction of the H-bonds in the cycle ("clockwise and counterclockwise"), produce distinct structural isomers upon complexation with 1MI, as shown in Figure 8. Calculations confirmed this distinction and argued against a W_3 chain complex because no minimum could be found for a chain structure. The clockwise and counterclockwise minima differ in binding energy by only 0.06 kcal/mol after ZPE correction (Table 1). The computed IR frequencies and intensities for the two isomers are shown in parts a and b of Figure 7. They faithfully reproduce the similarities and differences between the two experimental $1MI-W_3$ spectra (parts c and d of Figure 7), particularly in the spacing of the two π H-bonded OH stretch fundamentals appearing between 3600 and 3700 cm^{-1}. The presence of two π H-bonded OH stretches indicates that the W_3 cycles attach to 1MI at two sites, calculated to be near the C3 and C6 positions of 1MI. The methyl···OH_2 interaction seems to play a role in directing the W_3 structure above the 1MI π cloud as it did for $1MI-W_2$.

Figure 10 presents hole-burning scans in the $1MI-W_2^+$ mass channel. The IR laser was fixed at 3639 cm^{-1} in part b and 3646 cm^{-1} in part c. It was not possible to obtain a complete separation of the UV spectra of the two $1MI-W_3$ isomers because of the substantial overlap of the two congested spectra contaminating one another at most wavelengths. In particular, the scan in part c "burns out" both conformations of the W_3 cluster to some extent but still discriminates for isomer II over isomer I. Intensity differences between this scan and the cleaner hole-burning spectrum in part b could be used to assign all features in this region of the R2PI spectrum to the two isomers of $1MI-W_3$ described in the RIDIR analysis.

3. 3-Methylindole−(Water)$_1$. R2PI scans in the region of the $S_1 \leftarrow S_0$ origin of 3MI while monitoring the $3MI^+$ and $3MI-W_1^+$ mass channels are shown in Figure 11. Vibronic features are plotted relative to the monomer $S_1 \leftarrow S_0$ origin at 34 882 cm^{-1}. The previously assigned[23,26] origin of $3MI-W_1$ is shifted 236 cm^{-1} to the red of the monomer origin and is labeled in Figure 11b. The R2PI spectrum of $3MI-W_1$ is intriguing in several respects. First, many of the bands, which dominate the spectrum of the monomer, are missing or shifted in the complex. Second, the spectrum shows much more extensive and intense intermolecular structure than its $Ind-W_1$ analogue. Third, several of the bands, including the origin, are split or broadened. The possible implications of these unusual aspects of the R2PI spectrum for $^1L_a-^1L_b$ mixing will be taken up in the discussion section.

In addition, R2PI scans that extended more than 900 cm^{-1} to the red of the 3MI monomer origin in the W_1^+ and W_2^+ mass channels were recorded in searching for the expected features of larger water clusters. This lack of signal attributable to larger $3MI-W_n$ clusters has been noted in previous work also.[22,24,45]

The RIDIR spectrum for $3MI-W_1$ is shown in Figure 12b), recorded with the UV laser fixed on the $3MI-W_1$ $S_1 \leftarrow S_0$ origin (-236 cm^{-1}) while monitoring the $3MI^+$ mass channel. The spectrum of $3MI-W_1$ is almost indistinguishable from that of $Ind-W_1$, exhibiting an H-bonded N−H stretch (3442 cm^{-1}) and acceptor water symmetric (3652 cm^{-1}) and antisymmetric (3747 cm^{-1}) stretches within a few wavenumbers of their value in $Ind-W_1$. This confirms the structure of this cluster as N−H···OH_2. The dotted line in Figure 12b indicates the position of the NH stretch in 3MI monomer (3526 cm^{-1}), also recorded using RIDIR spectroscopy.

An IR−UV hole-burning scan in the $3MI-W_1^+$ mass channel (not shown) proves that all vibronic transitions in this mass channel can be attributed to the $3MI-W_1$ cluster.

IV. Discussion

A. Cluster Structures and IR Spectra. The structures of the indole−(water)$_n$ and methylindole−(water)$_n$ clusters sample a range of binding sites and H-bonding structures that can aid our understanding of the molecular-scale consequences of water solvation of indole.

1. Indole−Water and 3MI−Water: Water as H-Bond Acceptor from NH. The indole−water and 3MI−water complexes both form structures in which the water molecule acts as a H-bond acceptor from the N−H group of the indole ring. The indole−water complex is among the best characterized aromatic−water complexes, with a structure studied by rotationally resolved ultraviolet spectroscopy,[31] and with S_0- and S_1-state binding energies measured with impressive accuracy by two independent methods, including the ion photofragmentation scheme of Mons and co-workers reported in the adjoining paper.[42,46]

TABLE 4: Comparison of $S_0 \leftarrow S_1$ Origin Frequencies of Indole−(Water)$_n$ (n = 0, 2), 1-Methylindole−(Water)$_n$ (n = 0−3), and 3-Methylindole−(Water)$_n$ (n = 0, 1)

species	origin frequency[a]	relative wavenumbers[b]	Franck−Condon activity	structure
Ind	35 241	0	small	
Ind−W1	35 109	−132	small	N−H···OH_2
Ind−W2	34 789	−452	large	N−H···W_2···π
1MI	34 544	0	small	
1MI−W1	34 449	−95	moderate	π H-bond
1MI−W2	34 127	−417	large	π H-bound dimer
1MI−W3(I)	34 435	−109	large	π H-bound W_3 cycle
1MI−W3(II)	34 449	−95	large	π H-bound W_3 cycle
3MI	34 882	0	small	
3MI−W1	34 646	−236	large	N−H···OH_2

[a] Frequencies given in wavenumbers (cm^{-1}). [b] Origin frequencies given relative to their respective monomer origins.

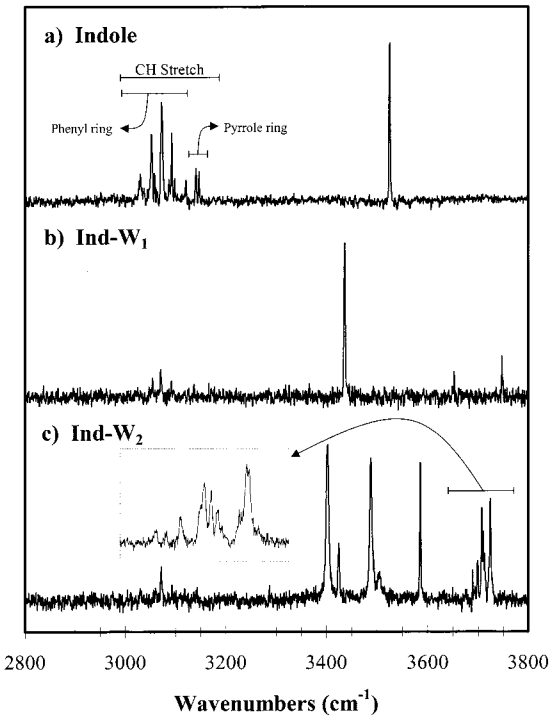

Figure 3. Resonant ion-dip infrared spectra of (a) indole monomer, (b) Ind−W_1, and (c) Ind−W_2. The free and π bound OH stretch region of Ind−W_2 is shown in an expanded view as an inset in part c. The wavenumber range of this inset is 3675−3750 cm^{-1}.

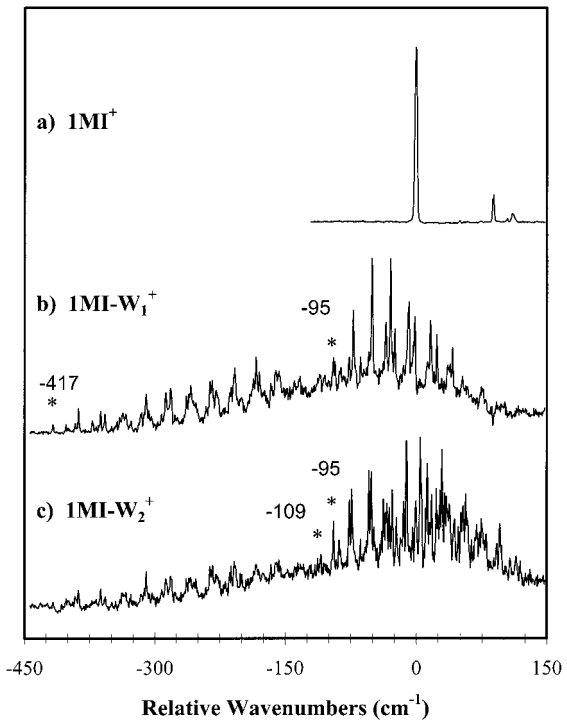

Figure 4. One-color resonant two-photon ionization spectra of the $1MI^+$ (a), $1MI-W_1^+$ (b), and $1MI-W_2^+$ mass channels in the $S_1 \leftarrow S_0$ origin region of 1MI. The zero of the relative wavenumber scale is the origin of 1MI (34 544 cm^{-1}). Origin transitions for the clusters are labeled and are confirmed by RIDIR and hole-burning spectra (see text).

The frequency shift of the XH stretch fundamental has been used for some time as an indirect measure of the strength of an XH···Y H-bond.[47] The magnitude of this frequency shift is correlated with a lengthening of the r_{XH} bond, a shortening of the R_{XY} distance, and an increase in the H-bond binding energy. While this correlation is a robust and useful one, there are comparatively few measurements of all these quantities in the gas phase, where solvent and matrix effects need not be considered. The present measurement of the frequency shift of the N−H stretch (−89 cm^{-1} in indole−water, −83 cm^{-1} in 3MI−water), when combined with the binding energy measurements of the adjoining paper,[42,46] completes the characterization of this complex and provides a benchmark for theory. The DFT Becke3LYP/6-31+G* calculations, after scaling, overestimate the shift by about 20% (−107 cm^{-1}).

2. Indole−(Water)$_2$: Hydrogen-Bonded Water Dimer Bridge. The structure for indole−W_2 incorporates the water dimer as a H-bonded bridge between two H-bonding sites: the NH group and the indole π cloud. Accumulating evidence from many groups[48−50] suggests that such bridges are a common feature in clusters for which the solute molecule has multiple H-bonding sites. Among the most dramatic examples of such bridges come from the recent results of Leutwyler and co-workers[50] on 7-hydroxyquinoline−W_n clusters in which water chains containing up to four water molecules connect the OH and N groups in 7-hydroxyquinoline.

It is intriguing to wonder whether such H-bonded bridges might be particularly efficient "conduits" for H atom or proton transfer between proton donor and acceptor sites. Furthermore, even in the absence of proton transfer, one might anticipate that the dynamics of vibrational energy transfer along such bridges should be unique and potentially important. The present results bear indirectly on such issues. The two lowest-frequency hydride stretch modes (3402 and 3488 cm^{-1}) involve concerted motion of the H-bonded N−H and O−H bonds, which make up the bridge. The lower-frequency band is a symmetric stretching mode that is about 70% (30%) on the NH (OH) stretch. It is this motion that in its extreme leads to concerted proton transfer along the bridge. The 3488 cm^{-1} band, on the other hand, is an antisymmetric combination of complementary NH−OH character. Not surprisingly, these bands are somewhat broader than

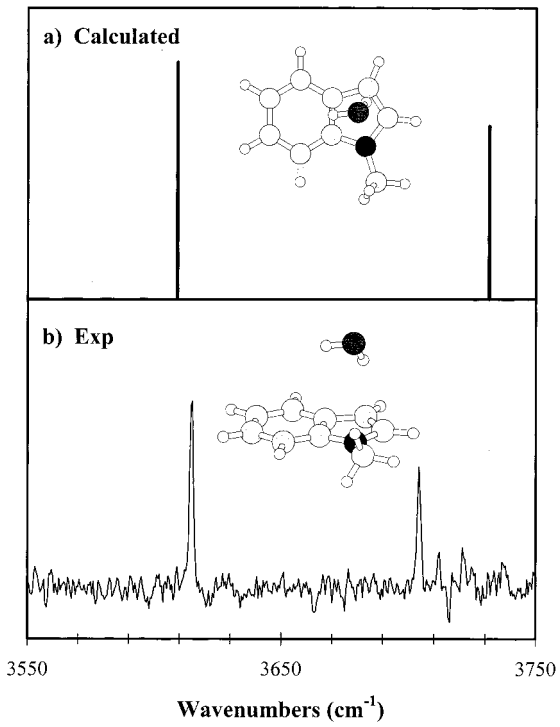

Figure 5. (a) Calculated, scaled OH stretch vibrational frequencies and intensities for 1MI−W_1. The scaling factor is 0.9775. Two orientations of the calculated structure for the complex are shown as insets. (b) Corresponding RIDIR spectrum of 1MI−W_1 with the R2PI laser tuned to the UV transition −51 cm^{-1} from the 1MI monomer origin in the R2PI spectrum of Figure 4b while monitoring the $1MI^+$ mass channel.

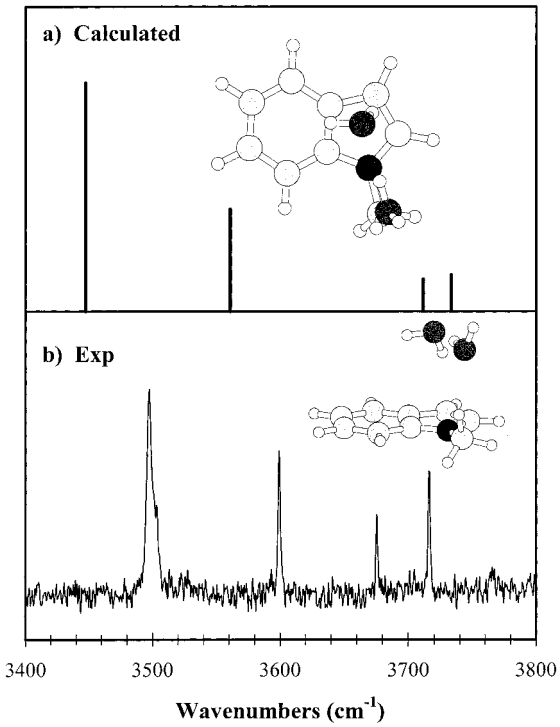

Figure 6. (a) Calculated, scaled OH stretch vibrational frequencies and intensities for 1MI−W_2. The scaling factor is 0.9775. Two orientations of the calculated structure for the complex are shown as insets. (b) Corresponding RIDIR spectrum of 1MI−W_2 with the R2PI laser tuned to the UV transition −208 cm^{-1} from the 1MI monomer origin in the R2PI spectrum of Figure 4b.

the OH stretch fundamentals not involved in the bridge, suggesting a somewhat stronger coupling to the bath of

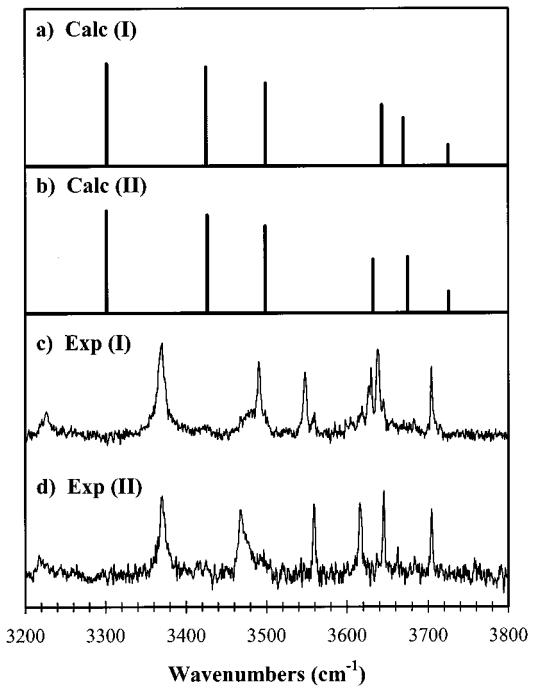

Figure 7. (a, b) Calculated, scaled OH stretch vibrational frequencies and intensities for the two cyclic 1MI−W_3 structures shown in parts a and b of Figure 8, respectively. The scaling factor for the vibrational frequencies is 0.9775. (c, d) Corresponding RIDIR spectrum of the two isomers of 1MI−W_3 with the R2PI laser tuned to the UV transitions −11 and +5 cm^{-1} from the 1MI monomer origin in the R2PI spectrum of Figure 4c.

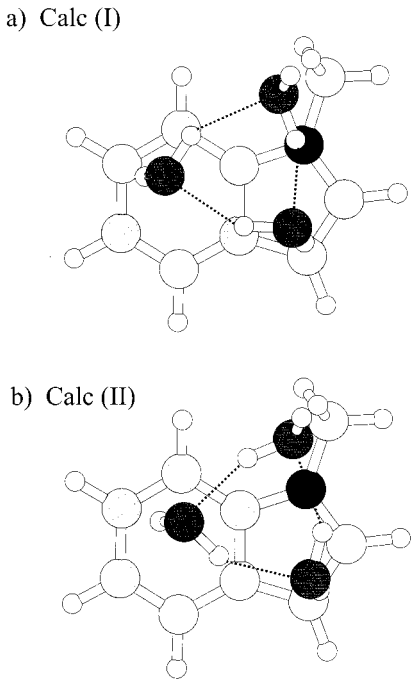

Figure 8. Calculated 1MI−W_3 structural isomers containing "clockwise" and "counterclockwise" W_3 H-bonded cycles. The structure shown in part a is calculated to be 0.03 kcal/mol more stable than its isomer in part b.

background states in the bridge vibrations. It will be interesting in future studies to track the changes in vibrational frequencies, intensities, and breadth of the "bridge" vibrations as a function of the length of the bridge, its structural strain, and the nature of the H-bond donor and acceptor sites that anchor the ends of the bridge.

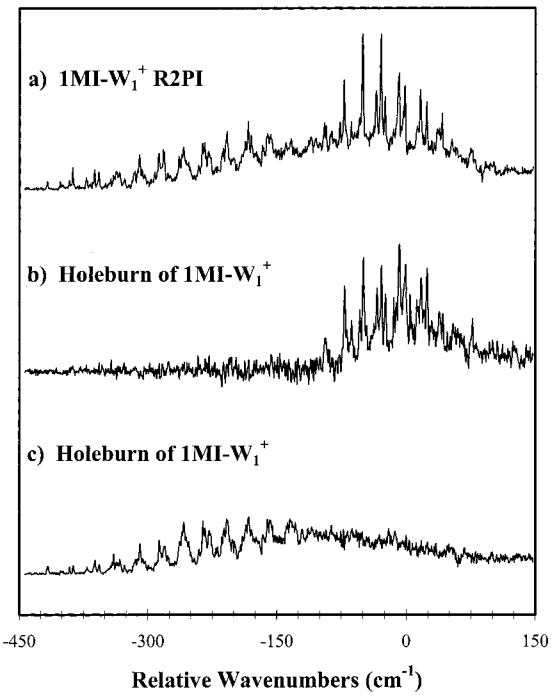

Figure 9. (a) One-color resonant two-photon ionization spectrum of $1MI-W_1^+$. The zero of this relative wavenumber scale is the $S_1 \leftarrow S_0$ origin of 1MI (34 544 cm^{-1}). (b) IR−UV hole-burning spectrum recorded with the infrared fixed at 3615 cm^{-1} (the symmetric OH stretch of $1MI-W_1$ from Figure 5b). (c) Corresponding IR−UV hole-burning scan with the IR fixed at 3599 cm^{-1} (the OH stretch of $1MI-W_2$ from Figure 6b).

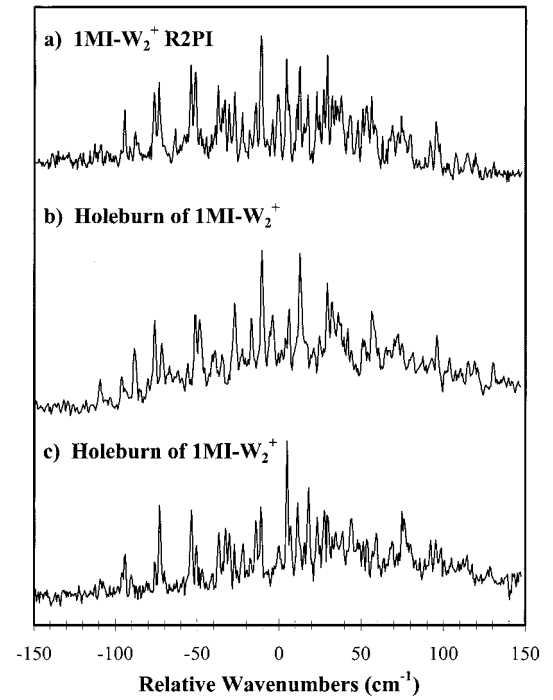

Figure 10. (a) One-color resonant two-photon ionization spectrum of the $1MI-W_2^+$ mass channel. The zero of this relative wavenumber scale is the $S_1 \leftarrow S_0$ origin of 1MI (34 544 cm^{-1}). (b) IR−UV hole-burning spectrum recorded with the infrared fixed at 3639 cm^{-1} (the symmetric OH stretch of $1MI-W_3$(I) from Figure 7c). (c) Corresponding IR−UV hole-burning scan with the IR fixed at 3646 cm^{-1} (the OH stretch of $1MI-W_3$(II) from Figure 7d).

3. 1MI−(Water)$_1$: Formation of a π H-Bond. The RIDIR spectrum of $1MI-W_1$ is quite clearly that of a π H-bonded water attached to the 1MI π cloud. As noted already, the experimental spectra are uninformative regarding the position of attachment of water on the 1MI π cloud. The DFT calculations predict that the preferred binding site is on the pyrrole ring above C3. Attempts to find a second minimum for $1MI-W_1$ over the phenyl ring were unsuccessful, with the water molecule minimizing to the C3 position even when placed initially over the phenyl ring.

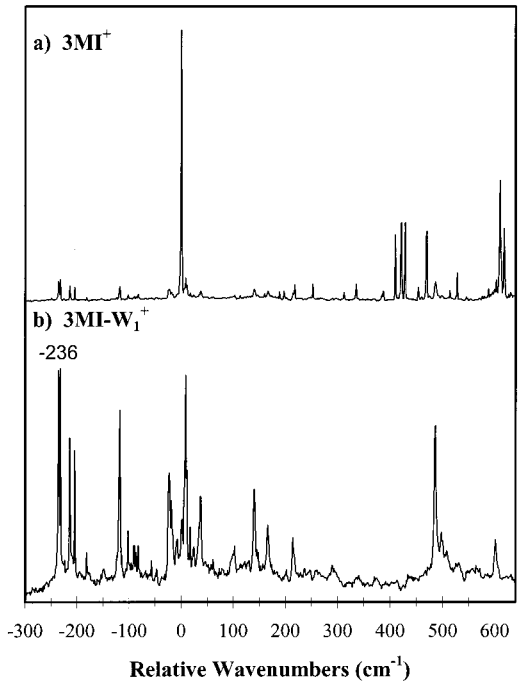

Figure 11. One-color resonant two-photon ionization spectra of the (a) $3MI^+$ and (b) $3MI-W_1^+$ mass channels in the $S_1 \leftarrow S_0$ origin region of 3MI. The zero of the relative wavenumber scale is the origin of 3MI (34 882 cm^{-1}). The origin of $3MI-W_1$ is located at an electronic frequency shift of −236 cm^{-1}.

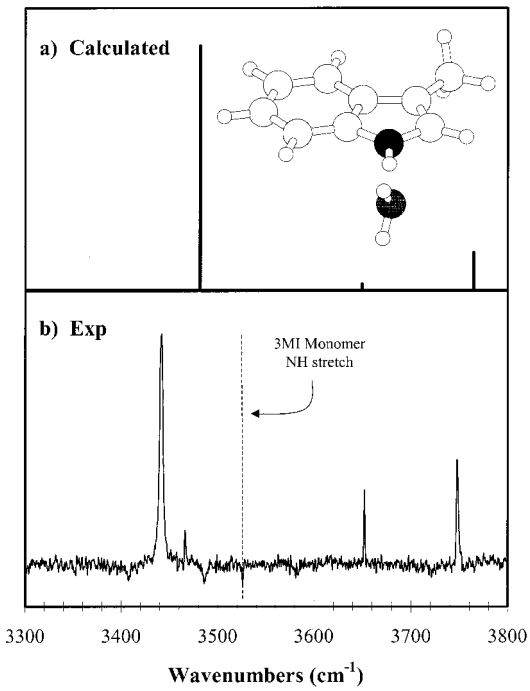

Figure 12. (a) Calculated, scaled OH stretch vibrational frequencies and intensities for $3MI-W_1$. The scaling factor is 0.9775. A picture of the calculated structure of $3MI-W_1$ is included. (b) Corresponding RIDIR spectrum of $3MI-W_1$ with the R2PI laser tuned to the UV transition −236 cm^{-1} from the 3MI monomer origin in the R2PI spectrum of Figure 10a.

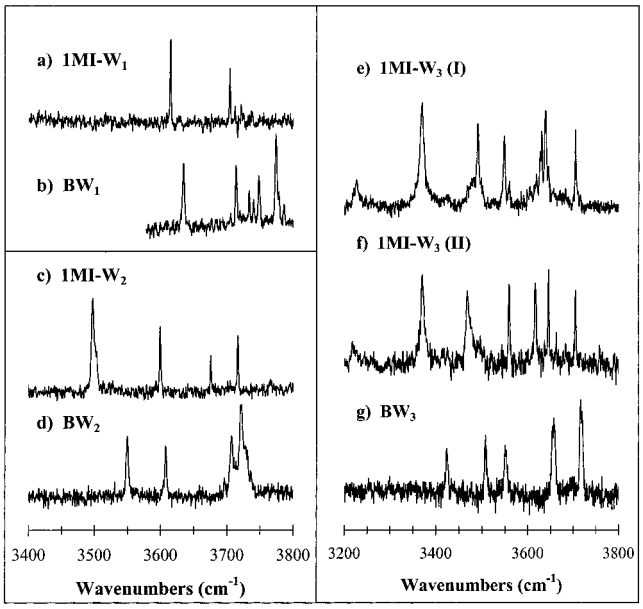

Figure 13. Comparison of the OH stretch RIDIR spectra of 1MI−W_n, $n = 1-3$, with the corresponding benzene−W_n clusters. The benzene−W_n RIDIR spectra are reproduced from ref 44.

The OH stretch infrared spectroscopy of 1MI−W_1 is fruitfully discussed by contrasting it with the analogous spectrum of benzene−(water)$_1$ recorded earlier by our group.[44] The two spectra are compared in parts a and b of Figure 13. In benzene−W_1, the π-bound water molecule undergoes large-amplitude motion even at the zero-point level. Because of the high symmetry of benzene's π cloud and the presence of two equivalent OH groups, the water molecule can reorient itself relative to benzene over a large range of angles with little cost in energy. The reorientation of the oscillating dipole that accompanies these motions produces large intensity in OH stretch−intermolecular combination bands involving these modes, as is obvious from the spectrum in Figure 13b.

By comparison, such combination bands are almost entirely missing from the spectrum of 1MI−W_1. Clearly, the asymmetry, strength, and corrugation of the intermolecular potential for the H-bond formed by water with the π cloud of 1MI largely quenches such large-amplitude motions, restoring the $\Delta v = 1$ infrared selection rules that typically govern infrared spectra.

The simple form of the RIDIR spectrum of 1MI−W_1, with its two sharp OH stretch transitions, clearly reveals the spectroscopic consequences of π H-bond formation. First, despite the strength of the π H-bond (which approaches that of the N−H···OH_2 H-bond),[42] the two OH stretch transitions are shifted down in frequency by only 40−50 cm^{-1} from their positions in free water. The magnitude of the hydride stretch frequency shift is often used as a measure of the strength of the H-bond. In keeping with this, the frequency shift of the OH stretch modes in 1MI−W_1 (−42 to −52 cm^{-1}; $D_0 = 4.10$ kcal/mol)[42] is about twice that in benzene−W_1 (−23 to −25 cm^{-1}; $D_0 = 2.44$ kcal/mol).[51] However, the magnitude of the frequency shift in 1MI−W_1 is much smaller than that for the N−H···OH_2 H-bond found in indole−W_1 (−89 cm^{-1}; $D_0 = 4.84$ kcal/mol), despite comparable binding energies. In the less conventional π H-bond, dispersion plays a much greater role in the binding, as discussed by Mons et al.[42] in the adjoining paper. It would appear that such dispersive interactions do not lead to the same shift in the OH stretch modes, yet they contribute substantially to the binding energy in the π H-bond.

Second, the splitting between the two OH stretch fundamentals in 1MI−W_1 (3704−3615 = 89 cm^{-1}) is about 10 cm^{-1} less than the splitting between symmetric and antisymmetric stretch modes in the free water monomer (3756−3657 = 99 cm^{-1}). The magnitude of this splitting reflects the magnitude of the intramolecular OH−OH coupling. Such a decrease in the intramolecular coupling is also observed in double-donor water molecules in benzene−(water)$_8$.[41] Here, we see that the formation of a π H-bond can produce effects that are comparable in magnitude.

Finally, the relative intensities of the symmetric and antisymmetric stretch modes in the RIDIR spectrum of 1MI−W_1 (Figure 5b) are about 1.5:1. The relative intensities of the OH stretch vibrations are among the most sensitive probes of H-bonding. For instance, the measured ratio of intensities of symmetric to antisymmetric stretch in indole−W_1 (where water acts as H-bond acceptor) is about 1:3. On the other hand, the analogous ratio of H-bonded OH stretch to free OH stretch intensities in a traditional OH···X H-bond is typically 10:1 in favor of the lower-frequency H-bonded OH stretch. We see that the π H-bond in 1MI−W_1 carries an intensity ratio that is between the two limiting cases.

4. 1MI−(Water)$_2$: π Bound Water Dimer. The structure deduced from the RIDIR spectrum of 1MI−W_2 is that of a π bound water dimer in which the acceptor water molecule in the dimer is H-bonded to the 1MI π cloud. The calculations point more specifically to this water dimer preferring the pyrrole site, with the high electron density at the C3 position serving as attachment point for the π H-bond. In the computed structure, the donor water in the water dimer sits over the methyl group of 1MI (Figure 6). This orientation of the water dimer antialigns its dipole with the ground-state dipole moment of 1MI. As indicated in Table 1, the resulting dipole moment of the 1MI−W_2 cluster is only 0.58 D, only 25% of the value of the 1MI monomer. This antialignment of the dipoles makes sense in maximizing the interaction of the water dimer with 1MI.

A comparison of the RIDIR spectrum of 1MI−W_2 with that of BW_2 is, once again, instructive. As shown in parts c and d of Figure 13c, there is a striking similarity in their IR spectra, as expected, given their similar π-bound water dimer structures. The lowest-frequency OH stretch transition in both spectra is largely localized on the water−water H-bonded OH. In 1MI−W_2, this transition is shifted down to 3498 cm^{-1}, corresponding to a frequency shift of −208 cm^{-1}. This is 52 cm^{-1} further than the corresponding band in BW_2, suggesting that there is a cooperative strengthening of the water−water H-bond by the π H-bond that is significantly greater in 1MI−W_2 than in BW_2. One would anticipate that this cooperative strengthening would also be reflected in a reduction in the O−O separation in the water dimer, but the magnitude of this effect must await high-resolution spectroscopy for verification.

The other three OH stretch transitions are assigned to the donor water's free OH stretch (3717 cm^{-1}) and the π bound acceptor molecule's symmetric (3599 cm^{-1}) and antisymmetric (3676 cm^{-1}) stretches. The separation between the latter two transitions has shrunk further to only 77 cm^{-1}, suggesting a further reduction in the intramolecular OH−OH coupling in the cooperatively strengthened π bound water.

5. 1MI−(Water)$_3$: Doubly π Bound, Chiral Cyclic Water Trimers. The RIDIR spectra for 1MI−W_3 have shown that there are two isomeric forms, both of which incorporate cyclic water trimer π-bound to 1MI. These structures provide an intriguing comparison with the free water trimer. In the free water trimer,

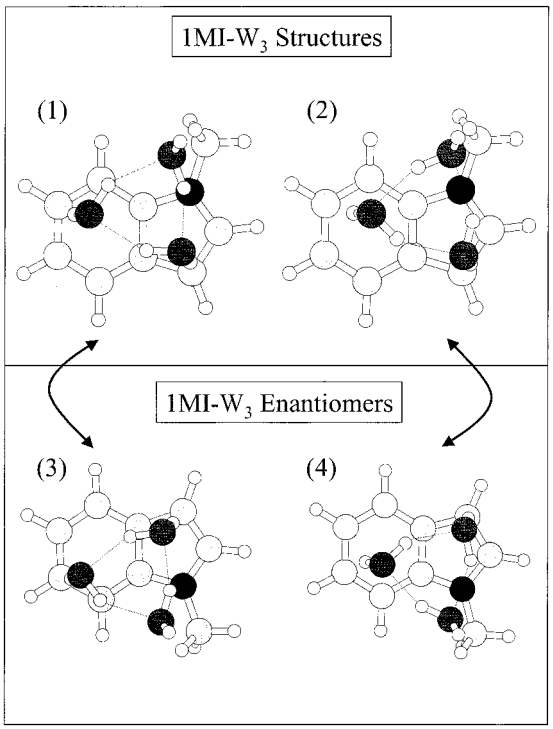

Figure 14. Illustration of the enantiomeric pairs (**3** and **4**) of the "clockwise" (**1**) and "counterclockwise" (**2**) isomers of the two 1MI−W_3 cycles.

the free OH groups point above or below the oxygen atom plane. The preferred structure is one in which two of the hydrogens point to one side of the oxygen atom plane (e.g., "up") while the third is on the other side of the plane ("down"). The up−down flipping coordinate presents a low-barrier tunneling route between identical minima, which has been studied in detail by several groups.[52−54] If this tunneling were quenched, one would have two chiral forms of the cyclic water trimer that could be viewed as "clockwise" and "counterclockwise" orientations for the H-bonds in the cycle. This resolution of two chiral forms of W_3 was in fact suggested to be the case in early work on the water trimer.[53]

In 1MI−W_3, the 1MI solute provides an asymmetric template for resolving these two chiral forms of the cyclic water trimer. As Figure 8 shows, the two isomers differ in precisely the way just mentioned, that is, in having different orientations of the H-bonds in the cycle relative to 1MI. As the calculations helped clarify, both isomers are "udd" (up−down-down) with respect to 1MI, with two π H-bonds formed with the π cloud of 1MI, one over the pyrrole ring and the other over the phenyl ring. In the RIDIR spectrum, these two π H-bonds are seen as distinct absorptions whose frequencies differ slightly in the two isomeric forms. These differences provided the most obvious spectroscopic distinction between the RIDIR spectra of the two isomers (parts c and d of Figure 7). The asymmetry of the 1MI surface has thus resolved the two chiral forms of the free water trimer. The binding of the two OH groups to the π cloud has quenched tunneling along the flipping coordinate, producing distinguishable isomers.

Interestingly, these isomers themselves come in enantiomeric pairs. As Figure 14 shows, reflection of structures **1** and **2** in the plane of the page produces mirror images **3** and **4** that cannot be superimposed on the original structures. Thus, there are two enantiomeric pairs of isomers present in the expansion. Of course, the enantiomers are not distinguishable from one another spectroscopically.

Other possible starting structures could be imagined, with the methyl group pointing down rather than up or with the pyrrole ring on the left rather than right. The structures produced when the "clockwise" and "counterclockwise" water trimers are brought up to these alternative starting geometries for 1MI are always interconvertible with the original four structures (Figure 14) via 2-fold rotations. The conclusion still holds, then, that there are two structurally distinct isomers of 1MI−W_3 that each exist as unresolved enantiomeric pairs.

This is an example of what must be a common occurrence in solution, namely, that solvent structures, which are similar in energy and easily interconverted in the absence of solute, become preferentially favored or disfavored in the vicinity of a solute. Here, we see two chiral forms of the water trimer being resolved by its binding to 1MI. While the energy difference between these two forms is admittedly small, one wonders whether the selective interactions between chiral solutes in solution might be mediated through or influenced by chiral solvating structures produced in the surrounding solvent.

The resolution of the two chiral forms of 1MI−W_3 begs the question regarding the presence of similar isomers in benzene−W_3. Given the 6-fold symmetry of the π cloud of benzene, it is possible that there is no distinction between binding clockwise and counterclockwise water trimers. No evidence for their presence at the vibronic level is found in either the ultraviolet or infrared spectra of benzene−W_3. However, it is also possible that the two forms are present but differ in such a subtle way that their ultraviolet transitions are unresolved at the resolution of the recorded R2PI spectra.[44] In this case, a rotationally resolved UV spectrum could potentially uncover the presence of the two isomers.

The two π H-bonded OH stretch fundamentals present in the spectra of 1MI−W_3 provide a first comparison of π H-bonds at the pyrrole and phenyl rings (Figure 8). The calculated forms of these normal modes predict the pyrrole interaction to be stronger (further red-shifted) than the phenyl π H-bond for both structures. The π H-bound O−H stretch at the pyrrole moiety is shifted 27 cm^{-1} to the red of the phenyl for calc I (9 cm^{-1} for exp I) and 43 cm^{-1} to the red for calc II (30 cm^{-1} for exp II).

The ring OH stretch fundamentals in 1MI−W_3 span a larger range and reach toward lower frequency than their counterparts in benzene−W_3 (Figure 13e-g). This likely reflects some cooperative strengthening of the water−water H-bonds induced by the stronger π H-bonding in 1MI−W_3. Also, both of the π interactions encountered in 1MI−W_3 appear to be stronger than the π interaction in BW_3.

B. Influence of Water Molecules on the ^1L_a−^1L_b Separation in Indole and Its Derivatives. The RIDIR spectra reported in this work have led to a firm assignment of the H-bonding topologies of several water-containing clusters of indole, 1MI, and 3MI. With these structures in hand, it is worth taking a closer look at the ultraviolet spectroscopy of the clusters in order to reassess the spectroscopic consequences of hydrogen bonding by water molecule(s) at the N−H and π cloud sites of indole. In so doing, one hopes to understand better the influence of water solvation on the relative energies, couplings, and nonradiative dynamics of ^1L_a and ^1L_b excited states of the indole chromophore.

There are several characteristic features of the ultraviolet spectroscopy and photophysics of indole derivatives and their water-containing clusters that have been associated with a selective lowering of the ^1L_a state relative to ^1L_b: (i) a large red shift in the position of the electronic origin; (ii) long

Franck−Condon progressions involving one or more intermolecular vibrations; (iii) red-shifted and broadened emission spectra; (iv) changes in the fluorescence lifetime. The large red shift in absorption and emission is the expected consequence of the unusual sensitivity of the ^1L_a state to stabilization by water molecule(s), with its large dipole moment (5.4 D).[3] The long FC progressions in excitation and the broadened emission spectra signal a response of the polar solvent (a solvent reorganization) to the large dipole moment change associated with formation of the ^1L_a excited state. The shortening of the fluorescence lifetime accompanies the opening of new nonradiative routes when ^1L_a and ^1L_b are in proximity.

While it is undoubtedly true that the ^1L_a state is more easily stabilized by water than ^1L_b, the magnitude of such lowering and its sensitivity to H-bonding to the π cloud were based on incorrect assignments for the π-bound isomers of indole−W_1 and 1MI−W_1.[22,26,27] Table 4 summarizes the revised assignments for the positions and shifts of the $S_1 \leftarrow S_0$ origins, the relative amount of Franck−Condon activity in the ultraviolet R2PI spectra, and the H-bonded structures deduced for the clusters from the RIDIR spectroscopy. The table shows no clear correlation between electronic shift, FC activity, and binding site, which would readily signal the turn-on of ^1L_a character. Indole−W_1 has water bound as H-bond acceptor at the N−H site of indole. Water complexation at the N−H site induces only a small shift in the electronic origin (-132 cm^{-1}) and little FC activity, in keeping with the expected insensitivity of either the ^1L_a or ^1L_b states to binding at this site. However, when the water molecule is moved up onto the indole π cloud in 1MI−W_1, the shift in the electronic origin is even smaller (-95 cm^1) and only moderate intermolecular FC activity is induced. Clearly, a single π H-bond with water is insufficient to turn on the expected signatures of ^1L_a lowering in 1MI.

Two clusters stand out as possessing both a large wavenumber shift and substantial FC activity: indole−W_2 and 1MI−W_2. While the latter structure is indeed a π-bound water dimer, indole−W_2 incorporates the water molecules as a H-bonded bridge between the N−H and π sites of indole. Finally, the two isomers of 1MI−W_3 incorporate the water trimer as π-bound cycles with large FC activity but small wavenumber shift.

It would appear, then, that in these clusters there is no clear evidence for a selective lowering of the ^1L_a state, at least as evidenced by the position or intermolecular vibronic structure of the observed spectra. In retrospect, given the magnitude of the $^1L_a-{}^1L_b$ gap in indole (1400 cm^{-1}) and 1MI (1100 cm^{-1}), it would seem unlikely that a single water molecule would be capable of changing the $^1L_a-{}^1L_b$ gap by such a sizable fraction of its total binding energy (1760 and 1530 cm^{-1} in the observed excited state, respectively).[42] Larger clusters would better overcome this energy difference, yet no clear evidence for such an occurrence exists.

An alternative explanation for the large red shift and substantial FC activity in the indole−W_2 and 1MI−W_2 ultraviolet spectra is that the observed excited-state levels are still ^1L_b in character, but the total binding energy of the cluster increases in S_1 compared to S_0 for other reasons. In the absence of solvent-induced electronic state coupling, the magnitude of the shift in the electronic origin of the cluster relative to the monomer measures the change in binding energy of the cluster following electronic excitation. Using indole−W_1 as an example, the -132 cm^{-1} shift in the $S_1 \leftarrow S_0$ origin relative to indole indicates that the N−H···OH_2 H-bond is stronger in S_1 than in S_0 by 132 cm^{-1}. It would seem that the N−H site of indole in the ^1L_b state is a better H-bond donor than it is in S_0. This was precisely the conclusion drawn from the structural analysis of the rotationally resolved spectrum of the $S_1 \leftarrow S_0$ origin.[31] By extension, one would surmise that the much larger shift in indole−W_2 (-452 cm^{-1}) could simply result from a greater cooperative strengthening of the N−H···OH and OH···OH H-bonds in S_1 over that in S_0.

The large FC activity observed in the $S_1 \leftarrow S_0$ spectrum of indole−W_2 also can appear for reasons other than ^1L_a coupling. The intermolecular structure is dominated by long progressions in a 34 cm^{-1} mode, which also appear in combination with a 48 cm^{-1} vibration. DFT calculations identify modes at 33 and 48 cm^{-1} in S_0 that involve a swinging of the H-bonded bridge along the π framework. It seems likely, then, that the excitation of analogous modes in S_1 simply reflects the strained nature of the H-bonded bridge formed by the water dimer in "reaching back" from the N−H site on the indole ring to form a weak H-bond with indole's π cloud. The electronic redistribution, which accompanies electronic excitation, would naturally induce motion along such bridge-swinging coordinates in response to the redistributed π cloud charge.

Similar arguments can be made for 1MI−W_2. In our discussion of the cluster structures, we noted already that the water dimer in 1MI−W_2 is oriented, according to the calculations, so that its dipole moment is antialigned with the dipole moment of the S_0 state of 1MI. Slater and Callis[55] have recently calculated the directions and magnitudes of the dipole moments for the ^1L_a and ^1L_b excited states of indole. According to these calculations (which compare favorably with experimental values for the magnitude of the dipole moment in ^1L_a and ^1L_b),[56] the dipole moment is about 10% greater in ^1L_b than in S_0 and points in the same general direction as in S_0. As a result, one anticipates a stronger interaction between the antialigned 1MI and water dipoles in the ^1L_b excited state than in S_0, leading to a red shift in the $S_1 \leftarrow S_0$ origin, as observed. The extensive intermolecular Franck−Condon activity observed in 1MI−W_2 is likely a consequence of the reorientation of the water dimer on the π cloud induced by the electronic excitation.

The case of 3MI−W_n clusters is potentially different. Here, the monomer already shows evidence of significant mixing of ^1L_b with ^1L_a within a few hundred wavenumbers of the $S_1 \leftarrow S_0$ origin.[24] Under such circumstances, the effects of binding even a single water molecule to 3MI could be significant. Indeed, as was mentioned in the results section, the 3MI−W_1 vibronic structure present in its ultraviolet spectrum shows little resemblance to the 3MI monomer. Not only is the intramolecular vibronic structure changed but the origin is split by 3.5 cm^{-1} and more extensive low-frequency intermolecular structure appears. It is hard to reconcile the splittings with changes in the barrier to methyl internal rotation, especially given the binding of water at the N−H site, spatially removed from the 3-methyl group. One could imagine that a coupling could exist between the internal rotation of the water and methyl groups, but again, the magnitude of the splittings (which increases to about 7 cm^{-1} in the intermolecular mode 21 cm^{-1} above the origin) seems too large to be accounted for in this way. Instead, it seems more likely to us that the changes in the spectrum of 3MI−W_1 are due to changes in the extent and type of mixing with ^1L_a induced by complexation to water.

Perhaps the most telling result of the present work for the ^1L_a state is one noted previously by other groups[22,24,45] and confirmed in this work; namely, that no R2PI signal could be obtained for clusters with more than one water molecule attached to 3MI. One wonders whether the lack of R2PI transitions ascribable to 3MI−W_n clusters with $n \geq 2$ is a signal that this

energy reversal has indeed occurred. The anticipated structure for 3MI−W_2 is the same one observed for indole−W_2, with the water dimer forming a H-bonded bridge between the N−H group and the π cloud of 3MI. If the true spectroscopic consequence of ^1L_a−^1L_b energy reversal is a sharp drop in the excited-state lifetime, then R2PI spectra of this cluster could be difficult to observe. Under these conditions, a direct absorption method, such as cavity ringdown, should be better suited to detection of the larger clusters. Such experiments are currently being pursued.

V. Conclusions

The clusters studied in this work sample several representative H-bonded structural types, including localized N−H···OH_2 donor−acceptor complexes, H-bonded water bridges between donor and acceptor sites (here, N−H donor and π acceptor), and π-bound water clusters reminiscent in their binding of the free water clusters. The present work is another in a fast-growing list of gas-phase cluster studies of water solvation of biologically relevant aromatics.[48−50] On the basis of this work, the representative H-bonding structures just noted appear to be widespread and potentially important.

Perhaps the most intriguing structural result in this work is the identification of two isomers of 1MI−W_3 that both incorporate a water trimer cycle but differ in the orientation of the H-bonds in the cycle relative to indole. The asymmetric template provided by the 1MI π cloud has resolved the two chiral isomers of cyclic W_3 that, in the absence of 1MI, can interconvert via the free H atom flipping tunneling coordinate.

The wider range of cluster structures sampled here has also led to a reevaluation of past deductions that even a single, π-bound water molecule can induce ^1L_a−^1L_b energy reversal in indole or 1MI. The ultraviolet spectroscopy of the indole−W_n and 1MI−W_n clusters near their $S_1 \leftarrow S_0$ origins can be explained entirely as ^1L_b state spectroscopy. This is the same deduction arrived at recently by Short and Callis[33] from their analysis of the two-photon excitation and dispersed fluorescence spectra of several indole−polar solvent complexes. ^1L_a mixing may be responsible for the unusual vibronic features observed for 3MI−W_1 and the decreased excited-state lifetimes of larger water-containing clusters.

Acknowledgment. The authors gratefully acknowledge the support of the National Science Foundation (9728636-CHE) for this work. T.S.Z. also thanks M. Mons and co-workers for sharing their results prior to publication, and P. Callis for useful discussions on the implications of the present work for ^1L_a−^1L_b coupling.

References and Notes

(1) Beechem, J. M.; Brand, L. *Ann. Rev. Biochem.* **1985**, *24*, 43.
(2) Demchenko, A. P. *Ultraviolet Spectroscopy of Proteins*; Springer-Verlag: New York, 1986.
(3) Lami, H.; Glasser, N. *J. Chem. Phys.* **1986**, *84*, 597−604.
(4) Vincent, M.; Gallay, J.; Demchenko, A. P. *J. Phys. Chem.* **1995**, *99*, 14931−14941.
(5) Strickland, E. H.; Horwitz, J.; Billups, C. *Biochemistry* **1970**, *9*, 4914−4921.
(6) Callis, P. R. *Methods Enzymol.* **1997**, *278*, 113.
(7) Gudgin, E.; Lopez-Delgado, R.; Ware, W. R. *J. Phys. Chem.* **1983**, *87*, 1559.
(8) Petrich, J. W.; Chang, M. C.; McDonald, D. B.; Fleming, G. R. *J. Am. Chem. Soc.* **1983**, *105*, 3824.
(9) Szabo, A. G.; Raynor, D. M. *J. Am. Chem. Soc.* **1980**, *102*, 554.
(10) Chang, M. C.; Petrich, J. W.; McDonald, D. B.; Fleming, G. R. *J. Am. Chem. Soc.* **1983**, *105*, 3824.
(11) Philips, L. A.; Webb, S. P.; Martinez, S. J., III.; Fleming, G. R.; Levy, D. H. *J. Am. Chem. Soc.* **1988**, *110*, 1352−1355.
(12) Teh, C. K.; Sipior, J.; Sulkes, M. *J. Phys. Chem.* **1989**, *93*, 5393.
(13) Fender, B. J.; Sammeth, D. M.; Callis, P. R. *Chem. Phys. Lett.* **1995**, *239*, 31−37.
(14) Callis, P. R. *J. Chem. Phys.* **1991**, *95*, 4230−4240.
(15) Elam, J. W.; Levy, D. H. *J. Chem. Phys.* **1997**, *106*, 10368−10378.
(16) Callis, P. R.; Vivian, J. T.; Slater, L. S. *Chem. Phys. Lett.* **1995**, *244*, 53−58.
(17) Serrano-Andres, L.; Roos, B. O. *J. Am. Chem. Soc.* **1996**, *118*, 185−195.
(18) Suenram, R. D.; Lovas, F. J.; Fraser, G. T. *J. Mol. Spectrosc.* **1988**, *127*, 472−480.
(19) Caminati, W.; Bernardo, S. D. *J. Mol. Struct.* **1990**, *240*, 253−262.
(20) Philips, L. A.; Levy, D. H. *J. Chem. Phys.* **1986**, *85*, 1327−1332.
(21) Berden, G.; Meerts, W. L.; Jalviste, E. *J. Chem. Phys.* **1995**, *103*, 9596−9606.
(22) Huang, Y.; Sulkes, M. *J. Phys. Chem.* **1996**, *100*, 16479−16486.
(23) Demmer, D. R.; Leach, G. W.; Wallace, S. C. *J. Phys. Chem.* **1994**, *98*, 12834−12843.
(24) Sammeth, D. M.; Siewert, S. S.; Spangler, L. H.; Callis, P. R. *Chem. Phys. Lett.* **1992**, *193*, 532−538.
(25) Remmers, K.; Jalviste, E.; Mistrik, I.; Berden, G.; Meerts, W. L. *J. Chem. Phys.* **1998**, *108*, 8436−8445.
(26) Tubergen, M. J.; Levy, D. H. *J. Phys. Chem.* **1991**, *95*, 2175−2181.
(27) Arnold, S.; Sulkes, M. *J. Phys. Chem.* **1992**, *96*, 4768−4778.
(28) Carney, J. R.; Hagemeister, F. C.; Zwier, T. S. *J. Chem. Phys.* **1998**, *108*, 3379−3382.
(29) Hager, J.; Ivanco, M.; Smith, M. A.; Wallace, S. C. *Chem. Phys. Lett.* **1985**, *113*, 503−507.
(30) Helm, R. M.; Clara, M.; Grebner, T. L.; Neusser, H. J. *J. Phys. Chem. A* **1998**, *102*, 3268−3272.
(31) Korter, T. M.; Pratt, D. W.; Kupper, J. *J. Phys. Chem. A* **1998**, *102*, 7211−7216.
(32) Muino, P. L.; Callis, P. R. *Chem. Phys. Lett.* **1994**, *222*, 156−160.
(33) Short, K. W.; Callis, P. R. *J. Chem. Phys.* **1998**, *108*, 10189−10196.
(34) Hager, J.; Wallace, S. C. *J. Phys. Chem.* **1984**, *88*, 5513−5519.
(35) Hager, J.; Ivanco, M.; Smith, M. A.; Wallace, S. C. *Chem. Phys.* **1986**, *105*, 397−416.
(36) Pratt, D. Personal communication.
(37) Gotch, A. J.; Zwier, T. S. *J. Chem. Phys.* **1992**, *96*, 3388−3401.
(38) Pribble, R. N.; Garrett, A. W.; Haber, K.; Zwier, T. S. *J. Chem. Phys.* **1995**, *103*, 531−544.
(39) Frisch, M. J.; Trucks, G. W.; Schlegel, H. B.; Gill, P. M. W.; Johnson, B. G.; Robb, M. A.; Cheeseman, J. R.; Keith, T. A.; Petersson, G. A.; Montgomery, J. A.; Raghavachari, K.; Al-Laham, M. A.; Zakrzewski, V. G.; Ortiz, J. V.; Foresman, J. B.; Peng, C. Y.; Ayala, P. Y.; Chen, W.; Wong, M. W.; Andres, J. L.; Replogle, E. S.; Gomperts, R.; Martin, R. L.; Fox, D. J.; Binkley, J. S.; Defrees, D. J.; Baker, J.; Stewart, J. P.; Head-Gordon, M.; Gonzalez, C.; Pople, J. A. *Gaussian 94*, revision B.3; Gaussian, Inc.: Pittsburgh, PA, 1995.
(40) Frisch, M. J.; Pople, J. A.; Binkley, J. S. *J. Chem. Phys.* **1984**, *80*, 3265.
(41) Gruenloh, C. J.; Carney, J. R.; Arrington, C. A.; Zwier, T. S.; Fredericks, S. Y.; Jordan, K. D. *Science* **1997**, *276*, 1678−1681.
(42) Mons, M.; Dimicoli, I.; Tardivel, B.; Piuzzi, F.; Brenner, V.; Millie, P. *J. Phys. Chem. A* **1999**, *103*, 9958.
(43) Muino, P. L.; Callis, P. R. *J. Chem. Phys.* **1994**, *100*, 4093−4109.
(44) Pribble, R. N.; Zwier, T. S. *Science* **1994**, *265*, 75−79.
(45) Hays, T. R.; Henke, W. E.; Selzle, H. L.; Schlag, E. W. *Chem. Phys. Lett.* **1983**, *97*, 347−351.
(46) Braun, J. E.; Grebner, T. L.; Neusser, H. J. *J. Phys. Chem.* **1998**, *102*, 3273−3278.
(47) Pimentel, G. C.; McClellan, A. L. *The Hydrogen Bond*; W. H. Freeman: San Francisco, CA, 1960.
(48) Held, A.; Pratt, D. W. *J. Am. Chem. Soc.* **1993**, *115*, 9708−9717.
(49) Dickinson, J. A.; Joireman, P. W.; Randall, R. W.; Robertson, E. G.; Simons, J. P. *J. Phys. Chem. A* **1997**, *101*, 513−521.
(50) Bach, A.; Leutwyler, S. *Chem. Phys. Lett.* **1999**, *299*, 381−388.
(51) Courty, A.; Mons, M.; Dimicoli, N.; Piuzzi, F.; Gaigeot, M. P.; Brenner, V.; Depujo, P.; Millie, P. *J. Phys. Chem. A* **1998**, *102*, 6590−6600.
(52) Geleijns, M.; Avoird, A. v. d. *J. Chem. Phys.* **1999**, *110*, 823−831.
(53) Pugliano, N.; Saykally, R. J. *Science* **1992**, *257*, 1937−1940.
(54) Schutz, M.; Burgi, T.; Leutwyler, S.; Burgi, H. B. *J. Chem. Phys.* **1993**, *99*, 5228−5238.
(55) Slater, L. S.; Callis, P. R. *J. Phys. Chem.* **1995**, *99*, 8572−8581.
(56) Chang, C. T.; Wu, C. Y.; Muirhead, A. R.; Lombardi, J. R. *Photochem. Photobiol.* **1974**, *19*, 347.